LETTER

Correlated Polyhedral Rotations in the Absence of Polarons during Electrochemical Insertion of Lithium in ReO$_3$

Nicholas H. Bashian,[†] Shiliang Zhou,[†] Mateusz Zuba,[‡] Alex M. Ganose,[¶,§,‖] Joseph W. Stiles,[†] Allyson Ee,[†] David S. Ashby,[⊥] David O. Scanlon,[¶,§,‖,#] Louis F. J. Piper,[‡,∇] Bruce Dunn,[⊥] and Brent C. Melot*,[†]

[†]Department of Chemistry, University of Southern California, Los Angeles, California 90089, United States

[‡]Department of Physics, Applied Physics and Astronomy, Binghamton University, Binghamton, New York 13902, United States

[¶]Department of Chemistry, University College London, 20 Gordon Street, London WC1H 0AJ, U.K.

[§]Diamond Light Source Ltd., Diamond House, Harwell Science and Innovation Campus, Didcot, Oxfordshire OX11 0DE, U.K.

[‖]Thomas Young Centre, University College London, Gower Street, London WC1E 6BT, U.K.

[⊥]Department of Materials Science and Engineering, University of California, Los Angeles, California 90095, United States

[#]The Faraday Institution, Quad One, Harwell Science and Innovation Campus, Didcot OX11 0RA, U.K.

[∇]Materials Science & Engineering, Binghamton University, Binghamton, New York 13902, United States

S *Supporting Information*

ABSTRACT: Understanding the structural transformations that materials undergo during (de)insertion of Li ions is crucial for designing high-performance intercalation hosts as these deformations can lead to significant capacity fade. Herein, we present a study of the metallic defect perovskite ReO$_3$ to determine whether these distortions are driven by polaronic charge transport (i.e., the electrons and ions moving through the lattice in a coupled way) due to the semiconducting nature of most oxide hosts. Employing numerous techniques, including electrochemical probes, operando X-ray diffraction, X-ray photoelectron spectroscopy, and density functional theory calculations, we find that the cubic structure of ReO$_3$ experiences multiple phase changes involving the correlated twisting of rigid octahedral subunits upon lithiation. This results in exceptionally poor long-term cyclability due to large strains upon lithiation, even though metallic character is maintained throughout. This suggests that phase transformations during alkali ion intercalation are the result of local strains in the lattice and not exclusively due to polaron migration.
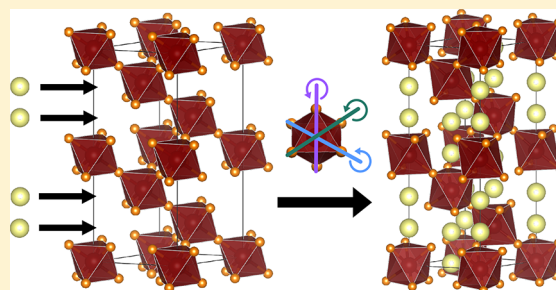
The reversible (de)insertion of Li ions into densely packed intercalation hosts is a complex process of fundamental importance to rechargeable batteries. As positively charged ions move in and out of a structure, redox-active transition-metal centers change their formal oxidation state and, in the process, adjust their bond lengths so as to maintain local charge neutrality.[1,2] These complex structural distortions generate substantial strain in the lattice that manifests itself as large changes to the unit-cell volume during cycling, which can result in cracking of the electrode and delamination from the current collector, ultimately shortening the life of the battery.[3,4] Developing a deeper understanding of these structural transformations and how they influence charge transport is therefore a critical open question for designing new intercalation hosts.

Our group recently demonstrated that the presence of rigid subunits within a structure necessitates the ability to undergo highly correlated polyhedral rotations in order to relieve the strain generated when ions are incorporated into the lattice. Contemporaneously, Banerjee and co-workers performed a detailed spectroscopic study on Li intercalation into V$_2$O$_5$ and identified a correlation between changes in the metal's first coordination shell and charge hopping through the lattice, suggesting the possibility that the rotations we had reported could be driven by polaronic charge transport.[5] Intrigued, we initiated a study of the *A*-site vacant perovskite ReO$_3$, one of

only a handful of metallic oxides that are known. The topology of the structure, illustrated in Figure 1, contains a perfectly
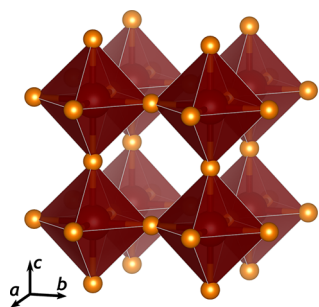

Figure 1. Cubic crystal structure of ReO_3 with oxygen and rhenium ions shown in orange and red, respectively.

cubic network of corner-sharing octahedra of ReO_6 with 90° and 180° O−Re−O and Re−O−Re bond angles, respectively, creating a three-dimensional network of interstitials that Cava, Murphy, and co-workers reported can accommodate up to two Li ions per formula units (i.e., Li_2ReO_3) when treated with *n*-BuLi.[6,7]

The coexistence of intrinsic metallic conductivity and pathways for facile ionic diffusion make ReO_3 a model system for exploring correlations between the transport of ions and electrons. While the open framework of ReO_3 has been heavily investigated in the past for its negative thermal expansion properties,[8,9] to our knowledge, there have been no studies that examine the role of structural flexibility on the performance of ReO_3 as an intercalation electrode in functioning Li-ion batteries. Herein, we characterize the electrochemical performance using operando synchrotron X-ray diffraction (XRD), density functional theory (DFT) calculations, and X-ray spectroscopy to better understand the fundamental mechanism for the (de)insertion of ions into the ReO_3. Although the metallic character of the starting phase might be expected to minimize lattice deformations resulting from polaron migration, we observe pronounced rotations of the Re octahedra during (de)insertion of Li. These tilting modes have a marked effect on the electronic structure of the material, eventually opening a small band gap in the fully lithiated Li_2ReO_3 end member. These distortions generate sufficient strain within the lattice to severely limit the reversible capacity over extended cycling, clearly demonstrating the importance of local structural distortions such as these for developing high-performance intercalation hosts.[10]

Several methods to prepare highly crystalline powders of ReO_3 have been reported.[11,12] The method of Chong et al. was chosen because of its ability to produce fairly monodispersed nanoparticles in a highly repeatable way, as illustrated in the inset of Figure 2.[13] Immediate heating of the solution of Re_2O_7 produced nanoparticles with an average size around 15 nm, and it was found that allowing the Re_2O_7 solution to sit on the bench prior to heating resulted in noticeably larger particles of ReO_3. The observation of lattice fringes in the transmission electron microscopy images, shown as the inset of Figure 2, clearly demonstrates that even very brief heating times were sufficient to yield highly crystalline particles of ReO_3. This is supported by the results of Rietveld refinement of the structure against synchrotron XRD patterns (Figure 2), which exhibit fairly sharp peaks with only very minor broadening of the reflections and no signs of any secondary phases. A
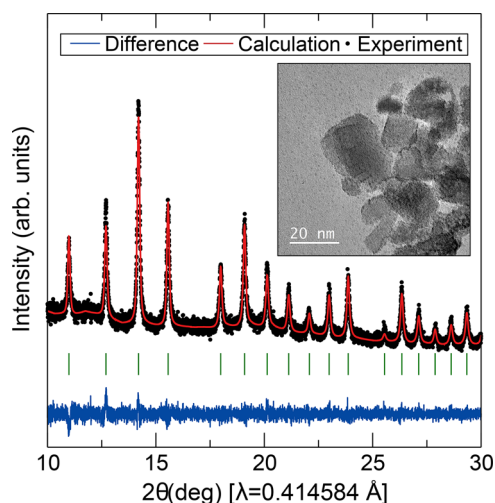

Figure 2. Results of the Rietveld refinement of the cubic structure against synchrotron XRD patterns of the nanoscale ReO_3 samples where $R_{Bragg} = 2.8\%$. Detailed results of the refinement can be found in Table S2.

microstructural analysis of the peak broadening performed within FullProf indicated an average particle size of 20 nm, in close agreement with the results of the microscopy. No significant differences were seen when cycling particles with larger sizes, so powders prepared in this way were used in all of the following discussion.

These powders were used to prepare film electrodes as described in the Experimental Details in the Supporting Information, and their galvanostatic performance was evaluated in standard Swagelok cells. During discharge, three distinct changes in slope can be seen at 2.5, 2.3, and 1.3 V, yet only the first and last feature are distinguishable on reversal, as shown in Figure 3a. The presence of such a polarization implies a kinetic barrier to either electron or ion transport. The metallic character of ReO_3 would seemingly preclude any issues with electronic transport, and therefore the polarization is likely related to sluggish Li-ion mobility or an asymmetric insertion process. Galvanostatic intermittent titration technique (GITT) experiments were therefore performed to determine how much of the polarization was due to nonequilibrium cycling conditions; however, a significant polarization is still seen even when the cell is allowed to fully relax (Figure S4).

The electrochemistry was further characterized using cyclic voltammetry in excess electrolyte in order to ensure (de)-insertion was not limited by mass transport effects. Powders of ReO_3 were deposited on strips of steel and characterized in a three-electrode configuration where an open circuit voltage near 3.4V was observed. Figure 3b shows the same three Faradaic peaks found in the galvanostatic cycling data between 1.0 and 4.0 V. Yet, when sweeping across the entire voltage window, a partially irreversible wave evolves below 1.5 V that corresponds to the onset of electrolyte reduction to form Li_2CO_3 on the surface of the cathode, as will be shown more clearly later.[14]

In order to gain insight into the mechanism for Li-ion intercalation into the perovskite framework, operando X-ray diffraction experiments were performed at the 17-BM line at Argonne National Lab. The use of synchrotron X-rays allows for the collection of high-intensity diffraction patterns during
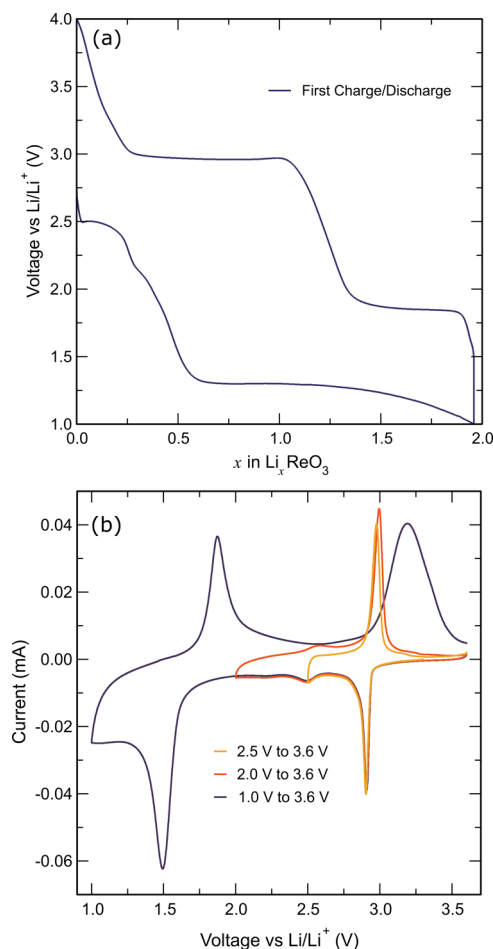
Figure 3. (a) Voltage vs composition of Li_xReO_3 during first cycle. (b) Cyclic voltammetry scans of ReO_3 microelectrodes collected at 1 mV s^{-1} against Li/Li^+ in a three-electrode cell within the glovebox.

Figure 4. Operando synchrotron X-ray diffraction patterns of ReO_3 throughout a complete discharge to Li_2ReO_3.

Figure 5. Illustration of the structural distortion that results in a twisting of the close-packed planes of oxygen in (a) ReO_3, (b) $LiReO_3$, and (c) Li_2ReO_3. Each structure is shown along the equivalent direction of the body diagonal within the cubic perovskite structure.

cell operation, showing clear correlations between electrochemical behavior and structural changes. Operando methods are important for ensuring the structural changes can be accurately correlated with distinct electrochemical features. Details of operando XRD experiments are provided in the Experimental Details within the Supporting Information. Figure 4 displays diffraction patterns that were collected every 15 min during a full discharge and charge cycle of Li_xReO_3 ($0 < x < 2.0$) at a C/10 rate.

Starting on discharge, the Bragg reflections maintain a relatively constant intensity but shift to higher angles for Li_xReO_3 ($0 < x < 0.35$), suggesting the cubic symmetry is maintained when small amounts of Li are inserted into the structure and that a solid solution can be obtained over this interval. Subsequently, the peaks associated with ReO_3 begin to lose intensity and new reflections that can be indexed to the hexagonal structure of Li_xReO_3 identifed by Cava et al. begin to grow.[7] Counterintuitively, this structural distortion leads to a *contraction* of the unit cell volume by approximately 5%, which is due to Li^+ ions being too small to fully fill the vacant *A*-site in the structure. Panels a and b of Figure 5 show that the transformation from the highly ordered cubic structure to the hexagonal phase is the result of octahedral tilting modes along the [111] direction of the cubic cell, while Figure S3 shows
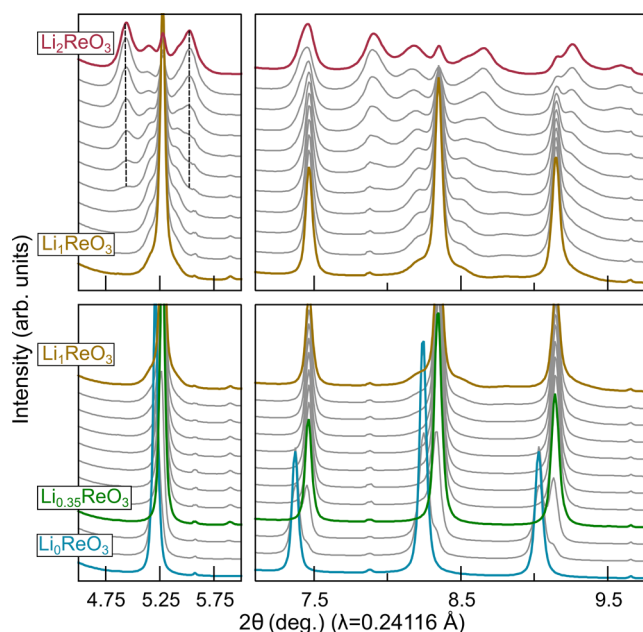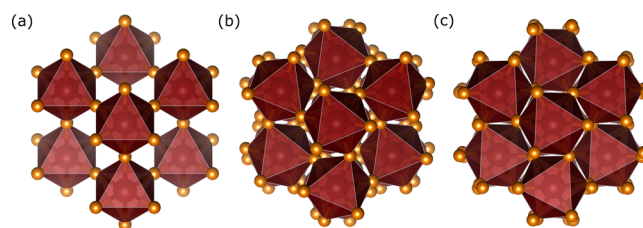
these rotations are accompanied by a contraction along the *c*-axis of the hexagonal cell.

As more Li is inserted, the peaks associated with the hexagonal phase remain essentially unchanged until approximately $x = 1.25$, at which point new reflections begin to evolve until complete lithiation at $x = 2.0$. This indicates that little structural rearrangement is required beyond the initial compression of the *A*-site pocket when only a single Li occupies each pocket. Yet, in order to insert beyond $x = 1.0$, the *A*-site must re-expand to allow two Li ions per pocket, which is clearly seen as the peak at 5.25° begins to evolve symmetric shoulders at 5.14° and 5.41° which continually increase their separation with increasing Li content. Interestingly, the Li_xReO_3 phase never seems to entirely disappear, suggesting an incomplete discharge during the operando measurement. Unfortunately, because of the close structural relationship and extensive peak overlap in the patterns, precise Rietveld refinement of individual patterns proved intractable.

On charging, changes in the diffraction patterns mirror those in the discharge process albeit over a slightly different compositional range, as shown in Figure S5. This can be seen in the peaks at 5.2°, 8.3°, and 9.1° that are visible from 0.5 > x > 2.0 compared to 2.0 < x < 1.25 on discharge. The reason for the asymmetry in the structural distortions can be

understood by examining Figures 5 and S3. Migration of Li into the cubic phase of ReO_3 proceeds through large vacancies in a highly symmetric close-packed lattice, whereas the octahedral rotations that produce the Li_2ReO_3 structure close these vacancies and block many of the pathways for Li-ion transport. It should, therefore, not be surprising that such a complex rearrangement of atoms to return to cubic symmetry would proceed through a different mechanism that involves a more correlated shuffling of ions across each interstitial.

More importantly, these distortions severely limit the long-term cycling stability, as shown in Figure 6, where only 40% of
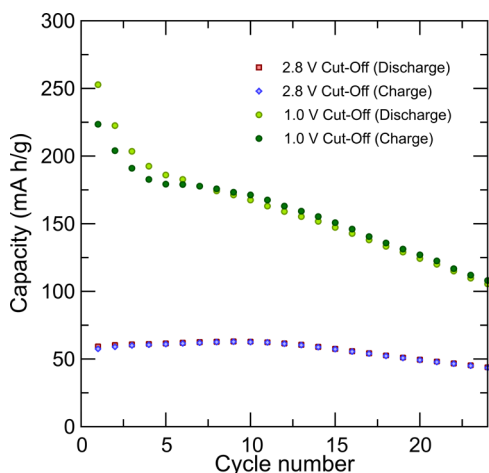

Figure 6. Charge and discharge capacity for a range of voltage cutoffs showing a severe loss of capacity when intercalating more than 0.35 equiv of Li ions into ReO_3.

the initial capacity is retained after 25 cycles when the lower cutoff voltage is set at 1.0 V. By setting the cutoff voltage to 2.8 V, which avoids these distortions by only inserting lithium into the cubic form of Li_xReO_3 ($x < 0.35$), the capacity can be stabilized over multiple cycles. This may be expected as structural deformations are well-known to produce particle cracking and dewetting from the current collector that can electrically isolate portions of the electrode and reduce the accessible capacity of the cell.[15−17] The severity of the effect is due to local strains as the corner-sharing octahedra rotate, bending the O−Re−O bond angle from 180° to 145° in Li_xReO_3 and 138° in Li_2ReO_3, corresponding a 23% change at full lithiation. The transformation to Li_xReO_3 also results in a 5% contraction of the unit cell, yet further lithiation to Li_2ReO_3 acts to cancel this contraction by expanding to nearly the same volume as the Li-free starting material in order to accommodate the two Li ions per A-site. Interestingly, such pronounced structural transformations are somewhat unexpected given that nanoscale powders usually suppress phase transformations.[18]

Having firmly established that the structure of ReO_3 distorts in a manner highly reminiscent to what has been reported for polyanionic intercalation hosts, the effect of these correlated rotations on the electronic structure was explored. As expected, hybrid density functional theory calculations indicate ReO_3 is metallic, with three doubly degenerate bands (Re 5d-t_{2g} character), crossing the Fermi level, with the two Re 5d-e_g bands found higher in energy (~4−6 eV above the Fermi level), in agreement with previous calculations.[19,20] In total, these six bands share a single electron, causing the Fermi level

to sit resonant within them. The density of states (DOS) and band structure of for ReO_3, $LiReO_3$, and Li_2ReO_3 are shown in Figure 7a−f. The orbital projected DOS clearly shows the edge of the valence band maxima to be entirely composed of Re 5d and O 2p orbitals, with the Re states dominating at the Fermi level.

Similar to ReO_3, the valence band of $LiReO_3$ is again composed of Re 5d and O 2p orbitals, with the metallic behavior being conserved despite the significant buckling of the Re−O bond angles. However, the rotations of the octahedra produce six significantly less disperse bands crossing the Fermi level in ReO_3 to split into two groups: the first consisting of two bands, spanning the energy range −0.6 to 1.0 eV, and the second consisting of four bands, spanning the energy range −2.0 to −0.3 eV. Further distorting the lattice to Li_2ReO_3 results in a medium band gap semiconductor, with an indirect band gap of 2.38 eV due to the full occupation of these six bands. These calculations indicate that Li_xReO_3 remains metallic for most values of x up until $x = 2.0$, which completely fills the valence band, strongly supporting the fact that the rotational distortions that occur on Li insertion are independent of any kind of polaron migration.

In order to experimentally corroborate the calculated DOS and further demonstrate that polaronic effects are not present during Li insertion, X-ray photoemission spectroscopy was used to evaluate the electronic structure of the phases. Figure 8a shows the Li 1s and Re 4f core regions of pristine and lithiated states of ReO_3. Pristine ReO_3 is expected to have a Re^{6+} oxidation state, with a $4f_{7/2}$ peak centered at 43.1 eV. The photoemission for ReO_3 displays additional peaks associated with surface Re^{7+}, because Re_2O_7 is the most thermodynamically stable phase and exists on the surface as Re^{7+} with its main peak at 45.5 eV.[21] Upon lithiation, the Re 4f shifts to lower binding energy and reaches a state indicative of having a Re^{4+} oxidation state (main $4f_{7/2}$ peak at 42.2 eV). In addition, the main Li 1s peak becomes present in the fully lithiated state. Because of the low discharge voltages, Li_2CO_3 and LiF contaminants contribute to this Li 1s signal. These assignments were based on the O 1s and F 1s core levels (see Figure S6). Given the fact that we can still see the Re 4f, we can estimate the surface contaminants have a thickness of ≤3 nm.

The valence band structure was measured for direct comparisons with the DFT calculations of the distorted Li_xReO_3 phases, with their band structures and density of states plotted in Figure 7. Figure 8b shows the valence band structure of Li_xReO_3 samples. In order to directly compare our experimental results with DFT, we accounted for the orbital cross sections and experimental broadening. The projected orbital density of states were weighted by the corresponding photoionization cross section.[22] Figure 8c shows the convoluted sum of orbital projections from DFT weighted by their corresponding photoionization cross-section convoluted with a Voigt profile (0.1 eV Lorentzian width, 0.5 eV Gaussian width) to match experimental resolution. Excellent agreement between the measured and calculated electronic structure of ReO_3 is observed; the 3−10 eV range is associated with primarily O 2p, and the topmost states up to the Fermi level are hybridized Re 5d-O 2p. As ReO_3 discharges, we see two additional features emerge at 4 and 9 eV along with increased intensity up to the Fermi edge, consistent with the DFT of $LiReO_3$. Upon discharge to 2 Li^+, we note differences between the XPS and DFT due to the aforementioned surface species. Figure 8b includes reference spectra of Li_2CO_3 and
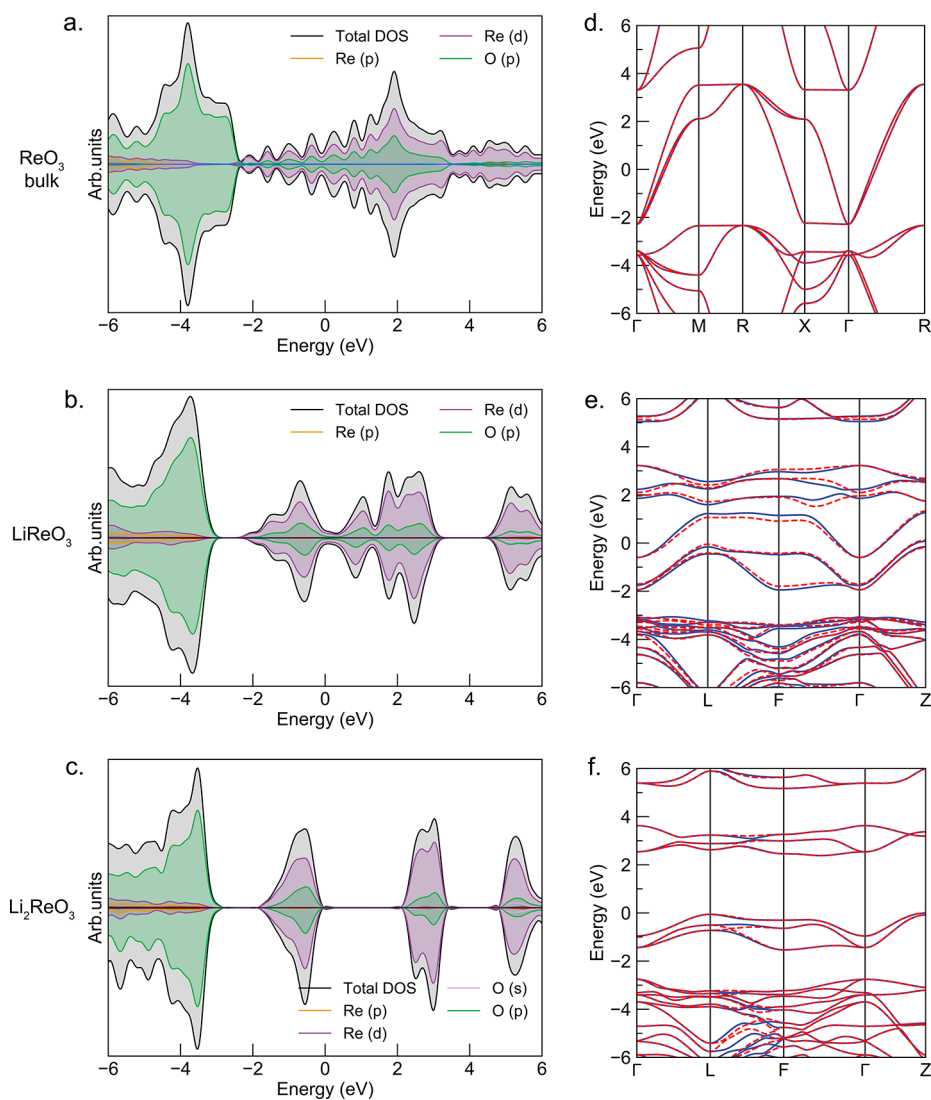
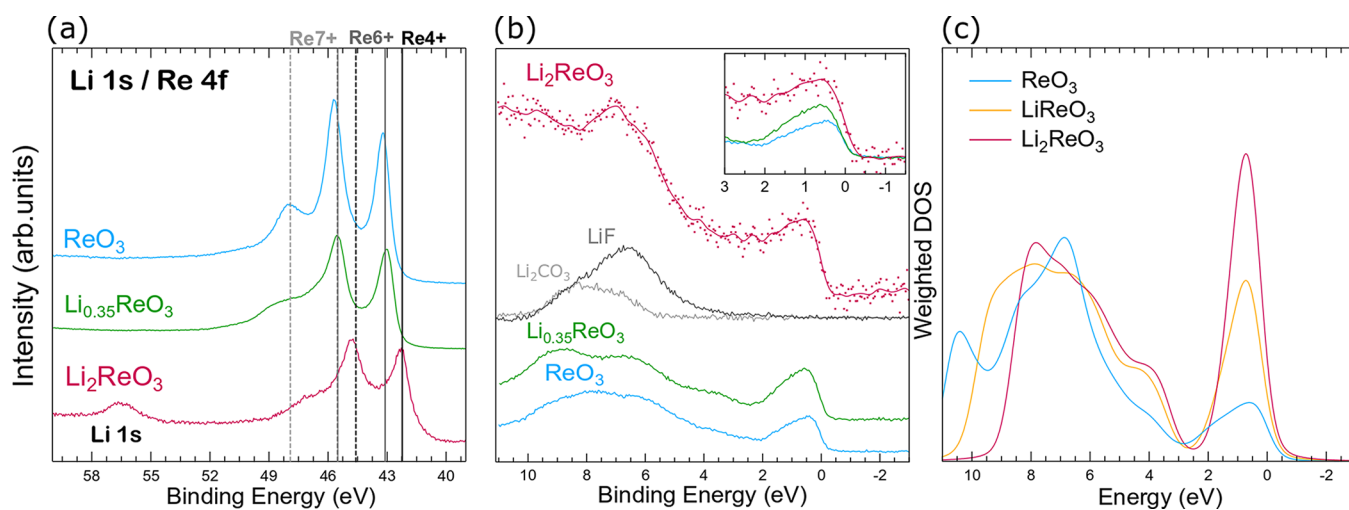Figure 7. (a−c) Densities of states and (d−f) band structure for ReO_3, $LiReO_3$, and Li_2ReO_3.

Figure 8. XPS of pristine ReO_3 and lithiated states ($Li_{0.35}ReO_3$ and Li_2ReO_3). (a) Re 4f core region with vertical line depicting Re oxidation state. (b) Valence band of O 2p and Re 5d hybridized regions with inset of Fermi level. (c) Weight and broadened density of states from DFT of ReO_3, $LiReO_3$, and Li_2ReO_3.

LiF, which are seen to increase the spectral weight in the 6−10 eV range. These surface species attenuate the Li_2ReO_3 signal

and partially account for the poorer statistics for Li_2ReO_3 despite the longer data acquisition time taken for this sample.

Despite these attenuating surface species, one still observes a very pronounced hybridized Re 5d-O 2p contribution in the XPS for Li_2ReO_3 (see the inset of Figure 8b), consistent with a fully occupied band. The poor photoemission signal of Li_2ReO_3 is consistent with the medium gap semiconducting character determined from the DFT calculations.

When all these results are combined, the metallic character of ReO_3 appears to be exceptionally robust toward bending of the O−Re−O bond angle. While in the metallic state, electron transport is fully decoupled from the motion of the intercalating ions, which appears to indicate that polaron migration is not driving the correlated rotations of the corner-sharing octahedra.

Using complementary electrochemical, spectroscopic, and structural characterization tools we have presented a detailed study on the mechanism of Li-ion insertion into ReO_3. While the open framework and metallic character of ReO_3 should, intuitively, allow it to exhibit exceptionally high performance as a cathode for Li-ion batteries, our results clearly show poor long-term cycling stability related to the highly correlated rotations of the corner-sharing perovskite octahedra. This work highlights the importance of understanding the underlying structural distortions that occur upon guest ion insertion during electrochemical cycling and, furthermore, demonstrates that the rotational distortions observed in insulating poly-anionic intercalation hosts do not appear to be purely caused by polaron migration. These structural distortions severely impede the reversible (de)insertion of Li into ReO_3 and would have to be suppressed in order for similar A-site vacant perovskite hosts to be effective electrode materials.

ASSOCIATED CONTENT

Ⓢ Supporting Information

The Supporting Information is available free of charge on the ACS Publications website at DOI: 10.1021/acsenergy-lett.8b01179.

> Experimental details, Rietveld refinement results, illustration of structural distortions, GITT measurements, operando XRD, and XPS measurements (PDF)

AUTHOR INFORMATION

Corresponding Author

*E-mail: melot@usc.edu.

ORCID Ⓘ

Shiliang Zhou: 0000-0003-3851-5176
David O. Scanlon: 0000-0001-9174-8601
Louis F. J. Piper: 0000-0002-3421-3210
Bruce Dunn: 0000-0001-5669-4740
Brent C. Melot: 0000-0002-7078-8206

Notes

The authors declare no competing financial interest.

ACKNOWLEDGMENTS

REFERENCES

(1) Zhou, S.; Barim, G.; Morgan, B. J.; Melot, B. C.; Brutchey, R. L. Influence of Rotational Distortions on Li^+- and Na^+-Intercalation in Anti-NASICON $Fe_2(MoO_4)_3$. *Chem. Mater.* 2016, 28, 4492−4500.

(2) Barim, G.; Cottingham, P.; Zhou, S.; Melot, B. C.; Brutchey, R. L. Investigating the Mechanism of Reversible Lithium Insertion into Anti-NASICON $Fe_2(WO_4)_3$. *ACS Appl. Mater. Interfaces* 2017, 9, 10813−10819.

(3) Bareño, J.; Shkrob, I. A.; Gilbert, J. A.; Klett, M.; Abraham, D. P. Capacity Fade and Its Mitigation in Li-Ion Cells with Silicon-Graphite Electrodes. *J. Phys. Chem. C* 2017, 121, 20640−20649.

(4) Feng, Y.; Dou, S.; Wei, Y.; Zhang, Y.; Song, X.; Li, X.; Battaglia, V. S. Preparation and Capacity-Fading Investigation of Polymer-Derived Silicon Carbonitride Anode for Lithium-Ion Battery. *ACS Omega* 2017, 2, 8075−8085.

(5) De Jesus, L. R.; Horrocks, G. A.; Liang, Y.; Parija, A.; Jaye, C.; Wangoh, L.; Wang, J.; Fischer, D. A.; Piper, L. F. J.; Prendergast, D.; Banerjee, S. Mapping Polaronic States and Lithiation Gradients in Individual V_2O_5 Nanowires. *Nat. Commun.* 2016, 7, 12022.

(6) Cava, R.; Santoro, A.; Murphy, D.; Zahurak, S.; Roth, R. The Structures of Lithium-Inserted Metal Oxides: $LiReO_3$ and Li_2ReO_3. *J. Solid State Chem.* 1982, 42, 251−262.

(7) Cava, R.; Santoro, A.; Murphy, D.; Zahurak, S.; Roth, R. The Structures of the Lithium Inserted Metal Oxides $Li_{0.2}ReO_3$ and $Li_{0.36}WO_3$. *J. Solid State Chem.* 1983, 50, 121−128.

(8) Rodriguez, E. E.; Llobet, A.; Proffen, T.; Melot, B. C.; Seshadri, R.; Littlewood, P. B.; Cheetham, A. K. The Role of Static Disorder in Negative Thermal Expansion in ReO_3. *J. Appl. Phys.* 2009, 105, 114901.

(9) Chatterji, T.; Henry, P. F.; Mittal, R.; Chaplot, S. L. Negative Thermal Expansion of ReO_3: Neutron Diffraction Experiments and Dynamical Lattice Calculations. *Phys. Rev. B: Condens. Matter Mater. Phys.* 2008, 78, 134105.

(10) Melot, B. C.; Scanlon, D. O.; Reynaud, M.; Rousse, G.; Chotard, J.-N.; Henry, M.; Tarascon, J.-M. Chemical and Structural Indicators for Large Redox Potentials in Fe-Based Positive Electrode Materials. *ACS Appl. Mater. Interfaces* 2014, 6, 10832−10839.

(11) Biswas, K.; Rao, C. N. R. Metallic ReO_3 Nanoparticles. *J. Phys. Chem. B* 2006, 110, 842−845.

(12) Nechamkin, H.; Kurtz, A. N.; Hiskey, C. F. A Method for the Preparation of Rhenium (VI) Oxide. *J. Am. Chem. Soc.* 1951, 73, 2828−2831.

(13) Chong, Y. Y.; Fan, W. Y. Facile Synthesis of Single Crystalline Rhenium (VI) Trioxide Nanocubes with High Catalytic Efficiency for

Photodegradation of Methyl Orange. *J. Colloid Interface Sci.* **2013**, *397*, 18−23.

(14) Quackenbush, N. F.; Wangoh, L.; Scanlon, D. O.; Zhang, R.; Chung, Y.; Chen, Z.; Wen, B.; Lin, Y.; Woicik, J. C.; Chernova, N. A.; Ong, S. P.; Whittingham, M.; Piper, L. F. J. Interfacial Effects in ϵ-Li$_x$VOPO$_4$ and Evolution of the Electronic Structure. *Chem. Mater.* **2015**, *27*, 8211−8219.

(15) Wang, H.; Jang, Y.; Huang, B.; Sadoway, D. R.; Chiang, Y. TEM Study of Electrochemical Cycling Induced Damage and Disorder in LiCoO$_2$ Cathodes for Rechargeable Lithium Batteries. *J. Electrochem. Soc.* **1999**, *146*, 473−480.

(16) Dokko, K.; Nishizawa, M.; Horikoshi, S.; Itoh, T.; Mohamedi, M.; Uchida, I. *In Situ* Observation of LiNiO$_2$ Single-Particle Fracture during Li-Ion Extraction and Insertion. *Electrochem. Solid-State Lett.* **2000**, *3*, 125−127.

(17) Jang, Y.-I.; Huang, B.; Wang, H.; Sadoway, D. R.; Ceder, G.; Chiang, Y.-M.; Liu, H.; Tamura, H. LiAl$_y$Co$_{1−y}$O$_2$ (R$\bar{3}$m) Intercalation Cathode for Rechargeable Lithium Batteries. *J. Electrochem. Soc.* **1999**, *146*, 862−868.

(18) Kim, H.-S.; Cook, J. B.; Tolbert, S. H.; Dunn, B. The Development of Pseudocapacitive Properties in Nanosized-MoO$_2$. *J. Electrochem. Soc.* **2015**, *162*, A5083−A5090.

(19) Mattheiss, L. Band Structure and Fermi Surface of ReO$_3$. *Phys. Rev.* **1969**, *181*, 987.

(20) Cora, F.; Stachiotti, M.; Catlow, C.; Rodriguez, C. Transition metal oxide chemistry: Electronic structure study of WO$_3$, ReO$_3$, and NaWO$_3$. *J. Phys. Chem. B* **1997**, *101*, 3945−3952.

(21) Greiner, M. T.; Rocha, T. C.; Johnson, B.; Klyushin, A.; Knop-Gericke, A.; Schlögl, R. The Oxidation of Rhenium and Identification of Rhenium Oxides During Catalytic Partial Oxidation of Ethylene: An In-Situ XPS Study. *Z. Phys. Chem.* **2014**, *228*, 521−541.

(22) Scofield, J. H. T. *Theoretical Photoionization Cross Sections from 1 to 1500 keV*; UCRL-51326; Lawrence Livermore Laboratory, 1973.